iScience

CellPress
OPEN ACCESS

Article

MiRNA post-transcriptional modification dynamics in T cell activation

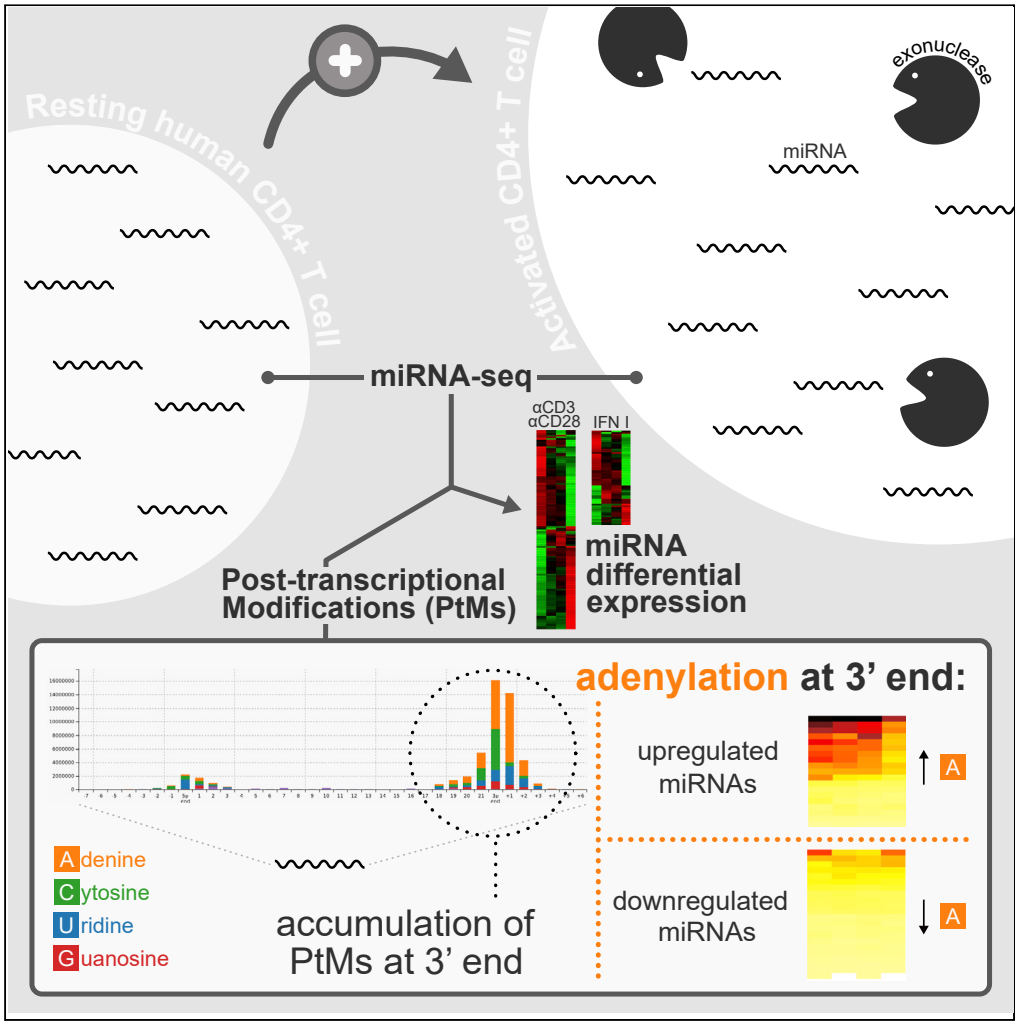

Ana Rodríguez-Galán, Sara G. Dosil, Manuel José Gómez, Irene Fernández-Delgado, Lola Fernández-Messina, Fátima Sánchez-Cabo, Francisco Sánchez-Madrid

fsmadrid@salud.madrid.org

Highlights

TCR and IFN I activation lead to miRNA differential expression in human CD4 T cells.

Upregulated miRNAs count with a stronger 3′ adenylation compared to those downregulated.

Cytosylation is a significant post-transcriptional modification in human T cells.

T cell activation triggers the expression of RNA degrading enzymes.

Rodríguez-Galán et al., iScience 24, 102530
June 25, 2021
https://doi.org/10.1016/j.isci.2021.102530

iScience

CellPress
OPEN ACCESS

Article

MiRNA post-transcriptional modification dynamics in T cell activation

Ana Rodríguez-Galán,[1,2] Sara G. Dosil,[1,2] Manuel José Gómez,[2] Irene Fernández-Delgado,[1,2] Lola Fernández-Messina,[1,2,3] Fátima Sánchez-Cabo,[2] and Francisco Sánchez-Madrid[1,2,3,4,*]

SUMMARY

T cell activation leads to extensive changes in the miRNA repertoire. Although overall miRNA expression decreases within a few hours of T cell activation, some individual miRNAs are specifically upregulated. Using next-generation sequencing, we assessed miRNA expression and post-transcriptional modification kinetics in human primary CD4+ T cells upon T cell receptor (TCR) or type I interferon stimulation. This analysis identified differential expression of multiple miRNAs not previously linked to T cell activation. Remarkably, upregulated miRNAs showed a higher frequency of 3′ adenylation. TCR stimulation was followed by increased expression of RNA modifying enzymes and the RNA degrading enzymes Dis3L2 and Eri1. In the midst of this adverse environment, 3′ adenylation may serve a protective function that could be exploited to improve miRNA stability for T cell-targeted therapy.

INTRODUCTION

MiRNAs are key modulators that fine-tune immune responses (Gracias and Katsikis, 2011; Lindsay, 2008; Mehta and Baltimore, 2016; Podshivalova and Salomon, 2013). During T cell activation, miRNA profile undergoes extensive changes, with a global downregulation of total miRNA levels occurring as early as 4 hr after activation (Bronevetsky et al., 2013). Beyond the overall picture of general reduction, some individual miRNAs stand out for their specific up- or downregulation, as shown by arrays, RT-qPCR and Northern Blot (Bronevetsky et al., 2013; Grigoryev et al., 2011; Gutiérrez-Vázquez et al., 2017; Jindra et al., 2010; Sousa et al., 2017; Teteloshvili et al., 2015; Wu et al., 2007). These studies, which evaluate mouse samples from 18 hr to 7 d and human samples from 2 to 7 d after activation, have been gathered together in a recent review (Rodríguez-Galán et al., 2018).

Little is known regarding the mechanisms that underlie these changes in the T cell miRNA landscape. Previous research from our laboratory pointed to 3′ uridine addition as a potential mechanism guiding miRNA turnover during T cell activation (Gutiérrez-Vázquez et al., 2017). Uridylation is a relatively common post-transcriptional miRNA modification. Next-generation sequencing (NGS) has identified not only nucleotide additions to the expected genomic miRNA sequences but also trimmings and substitutions (Ebhardt et al., 2009; Lee et al., 2010). Post-transcriptional modifications (PtMs) generate multiple variants of the same miRNA (isomiRs) that differ in their 5′, 3′ or internal modifications. PtMs modulate biogenesis, stability, and function (Gebert and MacRae, 2019; Neilsen et al., 2012; de Sousa et al., 2019). Several mechanisms elicit PtMs on the canonical miRNA sequence including: alternative processing by Drosha or Dicer, RNA editing and non-template nucleotide addition.

During miRNA biogenesis, Drosha cleaves the primary-miRNA transcript, generating a hairpin precursor-miRNA which is subsequently processed by Dicer, leading to the generation of a double-stranded miRNA duplex. Drosha and Dicer excisions are slightly flexible, thereby becoming a source of 5′ and 3′ isomiRs (Gu et al., 2012; Kim et al., 2017; Kwon et al., 2019; Starega-Roslan et al., 2011; Wu et al., 2009; Zhou et al., 2012; Zhu et al., 2018).

Other forms of PtMs derive from RNA editing which include conversion of adenosine (A) to inosine (I) by ADARs (adenosine deaminases acting on RNA) (Bazak et al., 2014; Nishikura, 2016; Tan et al., 2017; Yang et al., 2006); or deamination of cytidine (C) to uridine (U) by APOBECs (apolipoprotein B mRNA editing enzyme, catalytic polypeptide-like) (Blanc and Davidson, 2010; Rosenberg et al., 2011). Since I is

[1]Servicio de Inmunología. Hospital Universitario La Princesa, Instituto Investigación Sanitaria Princesa (IIS-IP), Universidad Autónoma de Madrid (UAM), 28006 Madrid, Spain

[2]Vascular Pathophysiology Area. Centro Nacional de Investigaciones Cardiovasculares (CNIC), 28029 Madrid, Spain

[3]CIBER de Enfermedades Cardiovasculares. Instituto de Salud Carlos III, 28029 Madrid, Spain

[4]Lead contact

*Correspondence: fsmadrid@salud.madrid.org

https://doi.org/10.1016/j.isci.2021.102530

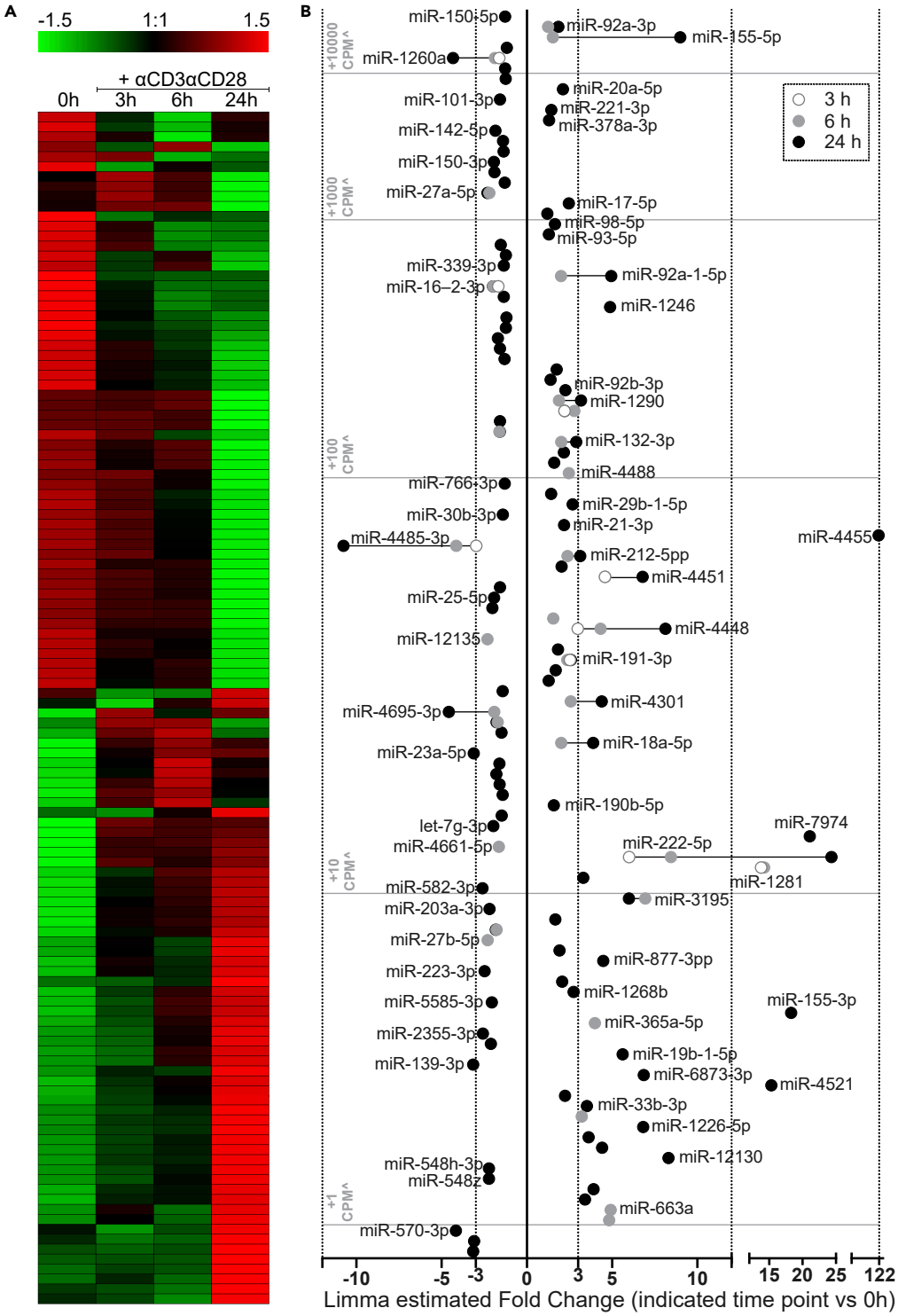

Figure 1. Differential miRNA expression 3h, 6h, and 24h after αCD3αCD28 stimulation of human primary resting CD4+ T cells

(A) The heatmap represents relative expression values for a non-redundant collection of differentially expressed miRNAs (adjusted p value <0.1), detected after stimulation with αCD3αCD28 for 3h, 6h, and 24hr.

Figure 1. *Continued*
(B) Limma estimated Fold Change of differentially expressed miRNAs at 3h, 6h, and 24hr compared to 0h. Representative miRNAs names are included, particularly those with higher fold changes. MiRNAs detected with higher CPM occupy top positions in Y axis (CPM^ = total sum of CPM detected at reference and represented time points; threshold bars indicate values at the bottom of each section). Table S1 contains 1B) raw data.

a guanosine (G) analog, A-to-I editing is equivalent to an A-to-G mutation. For miRNAs, A-to-I editing is well characterized (Li et al., 2018; Wang and Liang, 2018), whereas the physiological relevance of C-to-U modification is currently unknown.

Additional enzymes responsible for miRNA PtMs are terminal nucleotidyl transferases (TENTs). TENTs catalyze non-template additions of nucleotides mainly at the 3′ end (“tailing”) (Warkocki et al., 2018). TENTs are often flexible substrate-wise, but those with a preference toward adding adenosine are known as non-canonical poly(A) polymerases. Other TENTs promote the addition of uridine preferentially namely terminal uridyl transferases (TUTases). Uridylation and adenylation are the most typical 3′ end modifications across animal miRNAs (Burroughs et al., 2010; Chiang et al., 2010; Landgraf et al., 2007; Muller et al., 2014; Wyman et al., 2011). Multiple studies have explored these modifications and their consequences in detail. Conclusions often appear contradictory, likely due to the specific biological context, including different species, cell type or cellular compartment. For instance, GLD-2 (PAPD4/TENT2) 3′ monoadenylation seems to stabilize specific miRNA populations in human fibroblasts (D’Ambrogio et al., 2012) and miR-122 in the liver (Katoh et al., 2009). In mouse early embryos, 3′ mono- and oligoadenylation appears to protect certain miRNAs in a context of large degradation (Yang et al., 2016). However, PAPD5 (TENT4B/GLD4/TUT3) adenylates miR-21-5p on 3′, promoting its degradation by poly(A)-specific ribonucleases (Boele et al., 2014). In human monocytes, knocking down PAPD4 showed no overall effect of 3′ adenylation on miRNA stability, but adenylation instead altered miRNA effectiveness through reduction of their incorporation into the RNA-induced silencing complex (RISC, the complex where miRNAs induce mRNA degradation or inhibit their translation) (Burroughs et al., 2010). Uridylation also promotes diverse outcomes on miRNAs. Pre-let-7 miRNA can be uridylated at its 3′ end by TUT4 (ZCCHC11) or TUT7 (ZCCHC6) (Heo et al., 2009; Thornton et al., 2012). Lin28 (an RNA-binding protein) binds to pre-let-7 and favors oligouridylation (10-20 uridines), which inhibits subsequent Dicer processing and serves as a signal for Dis3L2 miRNA degradation (Chang et al., 2013; Heo et al., 2008, 2009; Thornton et al., 2012; Ustianenko et al., 2013). In the absence of Lin28, pre-let-7 undergoes monouridylation to pursue its maturation process (Heo et al., 2012). Let-7 promotes cell differentiation, and the regulatory mechanism triggered by Lin28 expression maintains pluripotency in stem cells (Büssing et al., 2008; Heo et al., 2009). Non-templated uridine addition also occurs on mature miRNAs, such as miR-26, which has been described to undergo 3′-uridylation by ZCCHC11 (terminal uridylyl transferase 4, TUT4) (Jones et al., 2009). MiR-26a and miR-26b uridylation has been shown to reduce their ability to repress IL-6 (Jones et al., 2009). In addition to Dis3L2, Eri1 is also a 3′ to 5′ exonuclease that exhibits a preference for uridylated RNA substrates (Hoefig et al., 2013).

In order to gain a mechanistic insight in the early changes occurring at the level of miRNA PtMs, we have studied the effect of stimulation of human primary CD4 T cells on miRNAs through NGS.

RESULTS

MiRNA modulation by αCD3αCD28

A total of 120 miRNAs were found to be differentially expressed (adjusted p value < 0.1, 62 upregulated and 58 downregulated) upon stimulation of resting human CD4 T cells with αCD3αCD28 for 3, 6 and 24 hr by NGS analysis [Figures 1A and 1B; Table S1]. Since large changes in total miRNA levels occur very early (Bronevetsky et al., 2013), 3 and 6 hr were chosen as intermediate points for our time course. MiRNAs from 5p and 3p arms were equally identified as differentially expressed with a total of 51% miR-5p and 49% miR-3p (those miRNAs without 5p or 3p included in the nomenclature were classified according to their localization of the mature sequence in miRbase). The most upregulated miRNAs (fold change indicated in brackets) at 24 hr were miR-4455 (122 x), miR-222-5p (24 x), miR-7974 (21 x), miR-155-3p (18 x), and miR-4521 (15 x) [Figure 1B]. Remarkably, miR-1281 showed a 14-fold change upregulation at 3 hr which was maintained at 6 hr but vanished at 24 hr. The most downregulated miRNAs at 24hr were miR-4485-3p (−11 x), miR-4695-3p (-5 x), miR-570-3p (-4 x), and miR-1260a (-4 x). Consistent with previous evidence, we also found downregulation of miR-150-5p, and miR-223-3p; while miR-155-5p, miR-17-5p, and miR-18a-5p

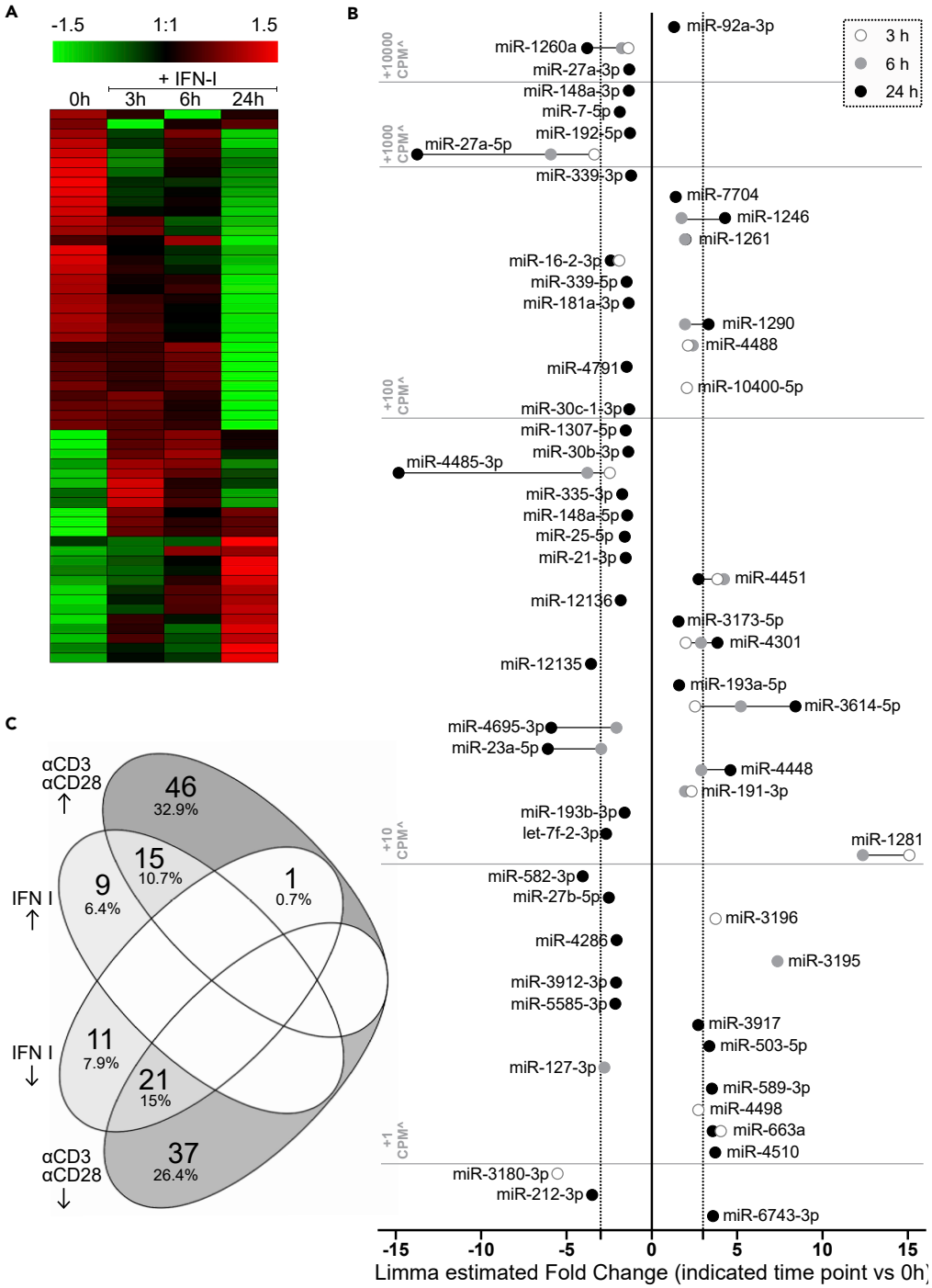

Figure 2. Differential miRNA expression 3h, 6h, and 24h after IFN I stimulation of human primary resting CD4+ T cells

(A) The heatmap represents relative expression values for a non-redundant collection of differentially expressed miRNAs (adjusted p value <0.1), detected after stimulation with IFN I for 3h, 6h, and 24hr.

(B) Limma estimated Fold Change of differentially expressed miRNA at 3h, 6h, and 24hr compared to 0h. MiRNAs detected with higher CPM occupy top positions in Y axis (CPM^ = total sum of CPM detected at reference and represented time points; threshold bars indicate values at the bottom of each section).

(C) Venn diagram with miRNAs differentially up- and downregulated by IFN I and αCD3αCD28. Table S2 contains 2B) raw data.

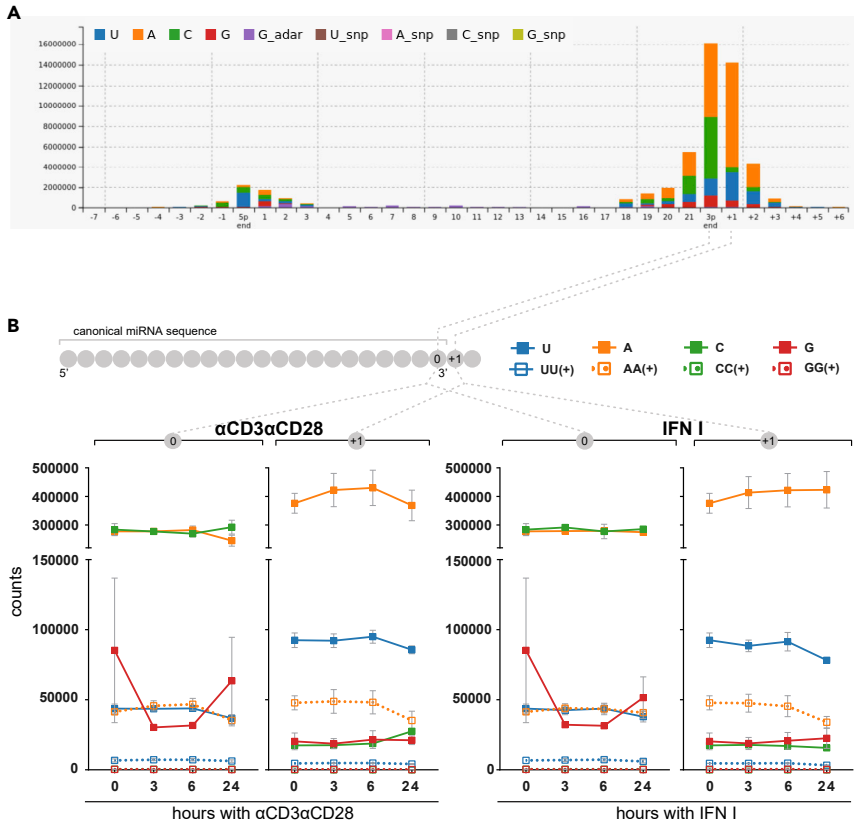

Figure 3. Post-transcriptional miRNA modifications: a global view

(A) Global post-transcriptional modifications (PtMs) profile for all 21 sequenced samples generated by Chimira.

(B) Kinetics of most abundant PtMs (mono-additions: U, A, C, G; and oligo-additions: ≥UU, ≥AA, ≥CC, ≥GG) at positions "3p-end" (0) and "3p-end + 1" (+1), in the population of 626 expressed miRNA species in unstimulated conditions and during activation with αCD3αCD28 (left) or IFN I (right). Mono-additions (solid squares) refer to the specific nucleotide on their own or followed by a different nucleotide, but not followed by the same nucleotide. Oligo-additions (empty squares) include PtMs with two or more equal nucleotides.

were upregulated (Rodríguez-Galán et al., 2018). We confirmed miR-1246 and miR-222-5p upregulation and miR-23a-5p and miR-27a-5p downregulation by qPCR [Figures S1A–S1D]. Ingenuity pathway analysis (IPA) indicated that differentially expressed miRNAs were mainly involved in processes related to cell development, growth, proliferation, and movement [Figure S2A]. Networks of predicted targets for the miRNAs with the highest up- and downregulation show a large overlapping, with 59 genes targeted by at least 2 of the 6 most upregulated miRNAs and 149, targeted by at least 2 of the 6 most downregulated [Figure S3A].

MiRNA modulation by IFN I

In a separate set, resting human CD4+ T cells were stimulated with type I interferon (IFN I). IFN I significantly altered the expression levels of 57 miRNAs (adjusted p value < 0.1): 24 miRNAs were upregulated, and 33 were downregulated [Figures 2A and 2B; Table S2]. Similar to αCD3αCD28 stimulation, 5p and 3p miRNAs were equivalently found as differentially expressed with a total of 49% miR-5p and 51% miR-3p. Compared with the data in Figure 1, we found that 37 miRNAs were common to the IFN I and αCD3αCD28 subsets (15 upregulated and 21 downregulated in both stimulations and 1 miRNA regulated in opposite directions) [Figure 2C]. The most upregulated miRNAs (fold change indicated in brackets) at 24 hr were miR-1281 (15 x, 3h), miR-3195 (7 x, 6h) and miR-3614-5p (8 x, 24hr). The most downregulated miRNAs at 24hr were miR-27a-5p (−14 x) and miR-4485-3p (−15 x) [Figures 2A and 2B]. miR-1246 upregulation and miR-23a-5p and miR-27a-5p downregulation were confirmed by qPCR [Figures S1A–S1D]. IPA revealed that most processes controlled by IFN I-regulated miRNAs were very similar to those observed for cells stimulated

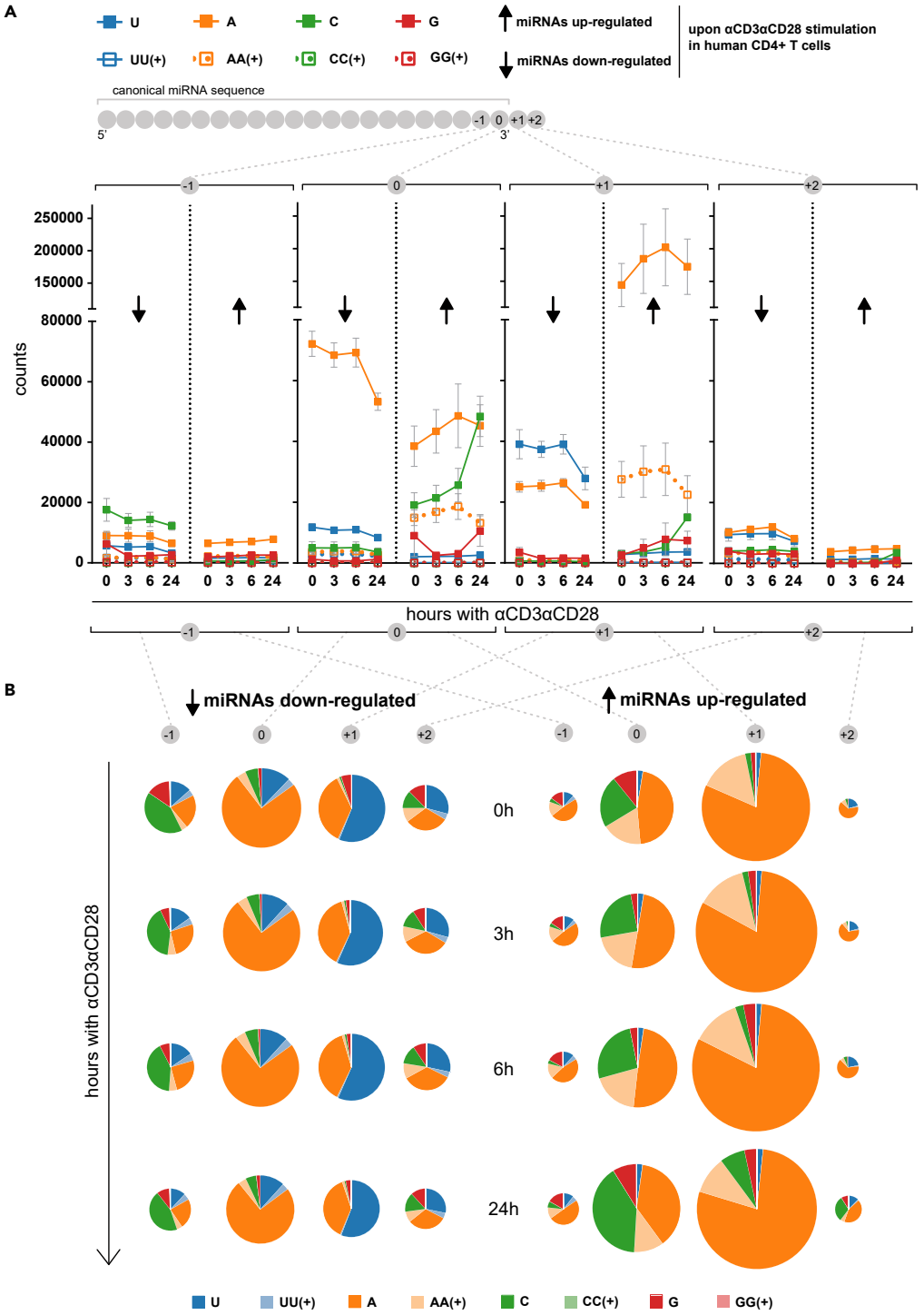

Figure 4. Kinetics of miRNA post-transcriptional modifications for αCD3αCD28 differentially expressed miRNAs

Kinetics of the most abundant PtMs (mono-additions: U, A, C, G; and oligo-additions: ≥UU, ≥AA, ≥CC, ≥GG) at positions "3p-end -1" (−1), "3p-end" (0), "3p-end + 1" (+1), and "3p-end + 2" (+2); for upregulated miRNAs (left) and downregulated miRNAs (right) with an adjusted p value <0.1. Mean and SEM (from three independent experiments) were plotted for each modification counts at specific positions across time points (A) and as pie charts whose area is proportional to the total number of counts for the specific position at indicated time points (B).

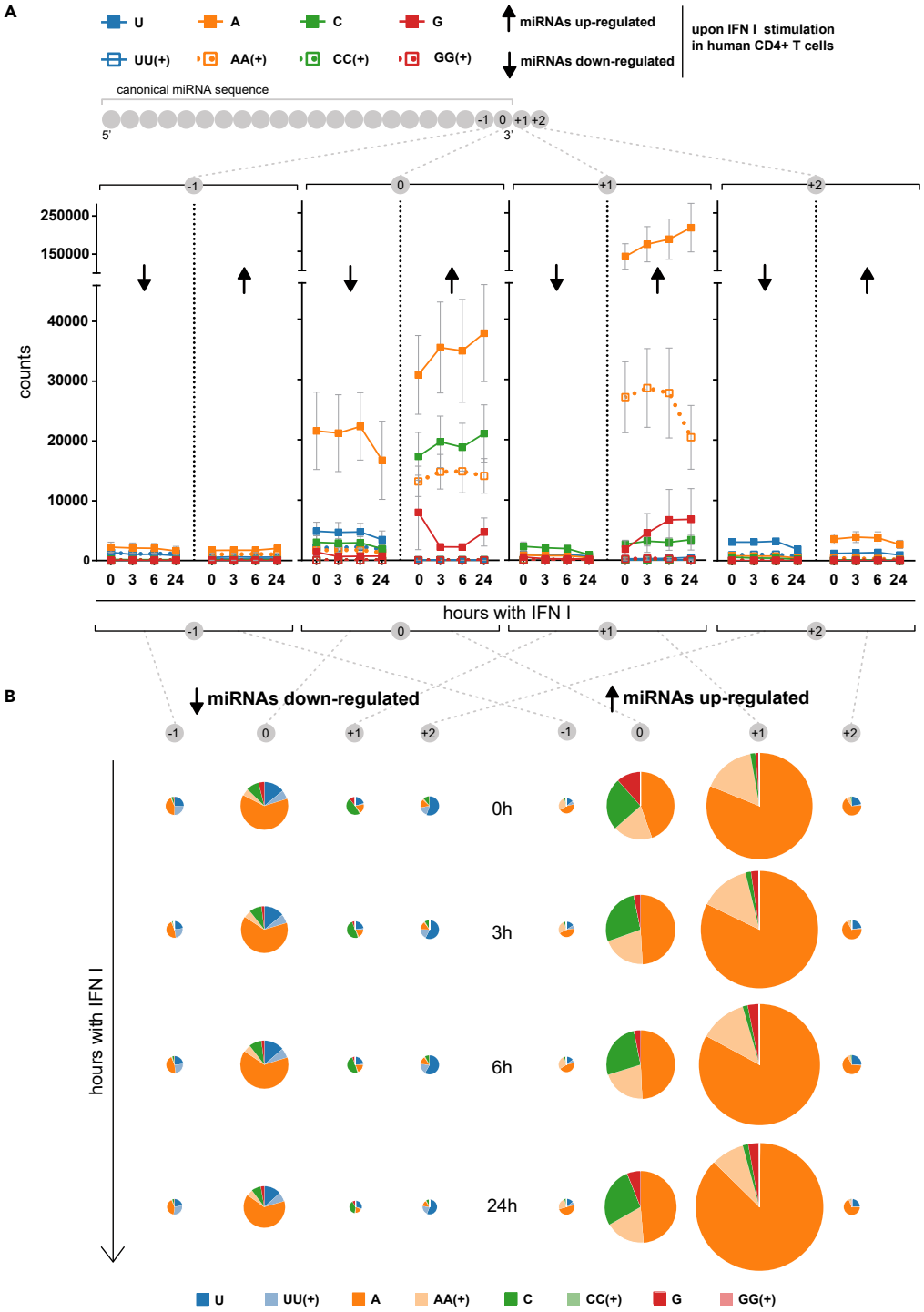

Figure 5. Kinetics of miRNA post-transcriptional modifications for IFN I differentially expressed miRNAs

Kinetics of most abundant PtMs (mono-additions: U, A, C, G; and oligo-additions: ≥UU, ≥AA, ≥CC, ≥GG) at positions "3p-end" (0) and "3p-end + 1" (1) and "3p-end + 2" (2), for upregulated miRNAs (left) and downregulated miRNAs (right) with an adjusted p value <0.1. Mean and SEM (from three independent experiments) were plotted for each modification counts at specific positions across time points (A) and as pie charts whose area is proportional to the total number of counts for the specific position at indicated time points (B).

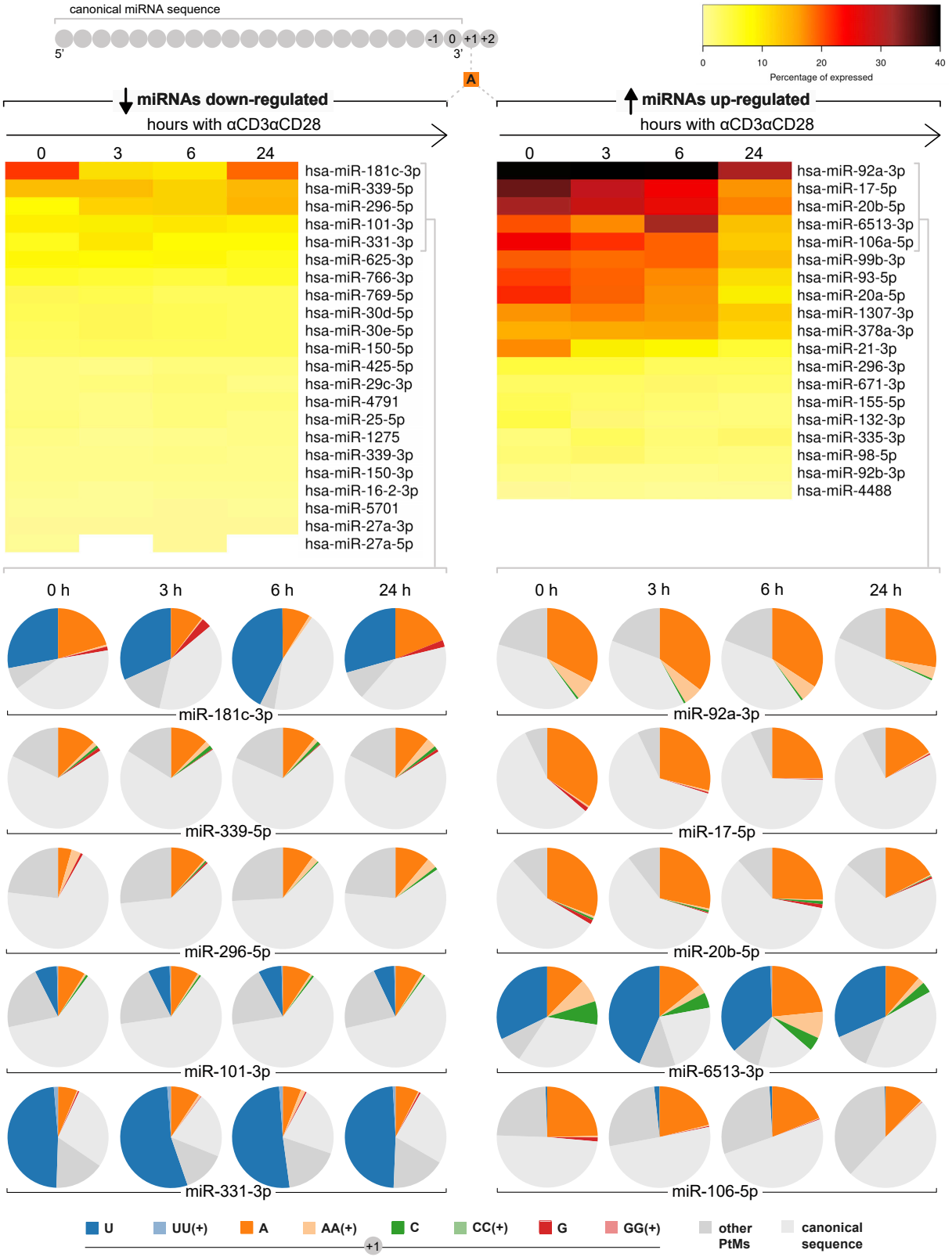
canonical miRNA sequence
5'
3'
-1
0
+1
+2
A
0
10
20
30
40
Percentage of expressed
miRNAs down-regulated
hours with αCD3αCD28
0
3
6
24
hsa-miR-181c-3p
hsa-miR-339-5p
hsa-miR-296-5p
hsa-miR-101-3p
hsa-miR-331-3p
hsa-miR-625-3p
hsa-miR-766-3p
hsa-miR-769-5p
hsa-miR-30d-5p
hsa-miR-30e-5p
hsa-miR-150-5p
hsa-miR-425-5p
hsa-miR-29c-3p
hsa-miR-4791
hsa-miR-25-5p
hsa-miR-1275
hsa-miR-339-3p
hsa-miR-150-3p
hsa-miR-16-2-3p
hsa-miR-5701
hsa-miR-27a-3p
hsa-miR-27a-5p
miRNAs up-regulated
hours with αCD3αCD28
0
3
6
24
hsa-miR-92a-3p
hsa-miR-17-5p
hsa-miR-20b-5p
hsa-miR-6513-3p
hsa-miR-106a-5p
hsa-miR-99b-3p
hsa-miR-93-5p
hsa-miR-20a-5p
hsa-miR-1307-3p
hsa-miR-378a-3p
hsa-miR-21-3p
hsa-miR-296-3p
hsa-miR-671-3p
hsa-miR-155-5p
hsa-miR-132-3p
hsa-miR-335-3p
hsa-miR-98-5p
hsa-miR-92b-3p
hsa-miR-4488
0 h
3 h
6 h
24 h
miR-181c-3p
miR-339-5p
miR-296-5p
miR-101-3p
miR-331-3p
miR-92a-3p
miR-17-5p
miR-20b-5p
miR-6513-3p
miR-106-5p
U
UU(+)
A
AA(+)
C
CC(+)
G
GG(+)
other PtMs
canonical sequence
+1

Figure 6. MiRNAs with significant adenylation at position 1 (αCD3αCD28)

Heatmaps include upregulated (right) and downregulated (left) miRNAs with significant adenylation at position 1, detected in αCD3αCD28 stimulation. Reads with adenine at position 1 are normalized to total reads, in order to visualize the frequency of adenylation for each miRNA. Pie charts are included below for the 5 miRNAs most adenylated within each group. These graphs show in color the percentage of reads with specific modifications at position 1, while reads with modifications at other positions and unmodified reads are depicted in gray.

through αCD3αCD28, mainly: cell development, movement, growth, and proliferation [Figure S2B]. Predicted targets show a more intense network overlapping among the 6 most downregulated miRNAs with 189 targets common to at least 2 miRNAs; while 52 genes would be targeted by at least 2 of the 6 most upregulated [Figure S3B].

Post-transcriptional modifications

A global assessment of PtMs indicated that miRNAs in our samples underwent extensive 3′-end modifications compared to their canonical sequences [Figure 3A]. Unexpectedly, C addition was highly represented in our samples at the most modified position: 0 or "3p end nucleotide". A and C modifications were similarly represented in this position, much more frequently than U and G [Figure 3A]. Modifications at 5′ end and ADAR editing (A to G) were detected on a very limited basis. According to the global profile, positions 0 (3p end) and +1 (3p end +1), were by far the most heavily modified, followed by positions −1 and +2 [Figure 3A]. For this reason, nucleotide modifications at the 3′ end were analyzed in greater detail in an attempt to discover specific sequences that could guide miRNA dynamics in T cells. PtMs patterns found in the 3′ end (positions −4 to 4) were evaluated (data not shown), indicating that the most common modifications across the different samples were: C, A, U, and G mono-additions, and A and U oligo-additions. "AU" was the most frequent multi-nucleotide modification, although sequences combining more than one nucleotide were clearly underrepresented. We also detected UAGU modifications at position −4, as well as AGU and AGUU at −3. We evaluated the presence of U, A, C, G and of UU+, AA+, CC+, GG+ (homopolymers of two or more equal nucleotides) at highly modified 3′-end positions. The results were conjoined for the different stimulation time points [Figure 3B]. Analyzed PtMs remained stable during activation and were clearly associated to a specific 3′ end position [Figure 3B].

To assess whether PtMs could be guiding the differential miRNA expression described in Figures 1 and 2, modifications at positions −1, 0, +1 and +2, were represented considering only data from miRNAs upregulated or downregulated, either upon αCD3αCD28 stimulation [Figures 4A and 4B] or IFN I [Figures 5A and 5B]. Upregulated miRNAs were more extensively modified, with the potential distinctive signature of high levels of A addition at +1 and C addition at 0 [Figures 4A, 4B, 5A, and 5B]. αCD3αCD28 downregulated miRNAs show reduced levels of these specific modifications and a marked presence of U additions, mostly at +1 [Figures 4A and 4B]. Adenine additions at position +1 were much higher in upregulated miRNAs with counts of A mono-additions around 140000-210000, while downregulated miRNAs counts did not go beyond 30,000 in αCD3αCD28 stimulation [Figure 4A] or 2000 in IFN I [Figure 5A]. Additions of two or more adenines were also a specific signature of upregulated miRNAs at 0 and +1 [Figures 4A and 5A].

To gain a better understanding of the most abundant modifications in upregulated miRNAs, we identified the individual miRNAs exhibiting higher adenylation at position 1 and cytosylation at position 0 [Figures 6, 7, S4, and S5]. A higher number of modified miRNAs were found after αCD3αCD28 stimulation [Figures 6 and 7], than in IFN I [Figures S4 and S5]. A group of miRNAs was found to be significantly cytosylated [Figures 7 and S5]. Nevertheless, miR-3195 on its own seems to account for the differential accumulation of cytosylation in upregulated miRNAs. Remarkably, a higher frequency of adenylation was found in upregulated miRNAs [Figures 6 and S4]. MiR-92a-3p, the upregulated miRNA with higher expression both in αCD3αCD28 [Figure 1] and IFN I [Figure 2] stimulations, counts with 31-42% of reads with an adenine at position 1 in all evaluated time points. In αCD3αCD28 stimulation, we have identified a group of upregulated miRNAs which present a higher frequency of adenylation [Figure 6].

Dis3l2, Eri1, TUT4, and TUT7 regulation upon T cell activation

Next, we evaluated the expression kinetics of four proteins related to RNA metabolism: TUT4 and TUT7 (terminal uridylyl transferases), and Dis3L2 and Eri1 time lengths (exonucleases that preferentially degrade uridylated RNA (Chang et al., 2013; Hoefig et al., 2013; Ustianenko et al., 2013)). For these experiments, we stimulated human CD4+ T cells from eight human healthy donors with αCD3αCD28 during various times up to 48 hr. A significant average upregulation was found after activation for all evaluated enzymes [Figures

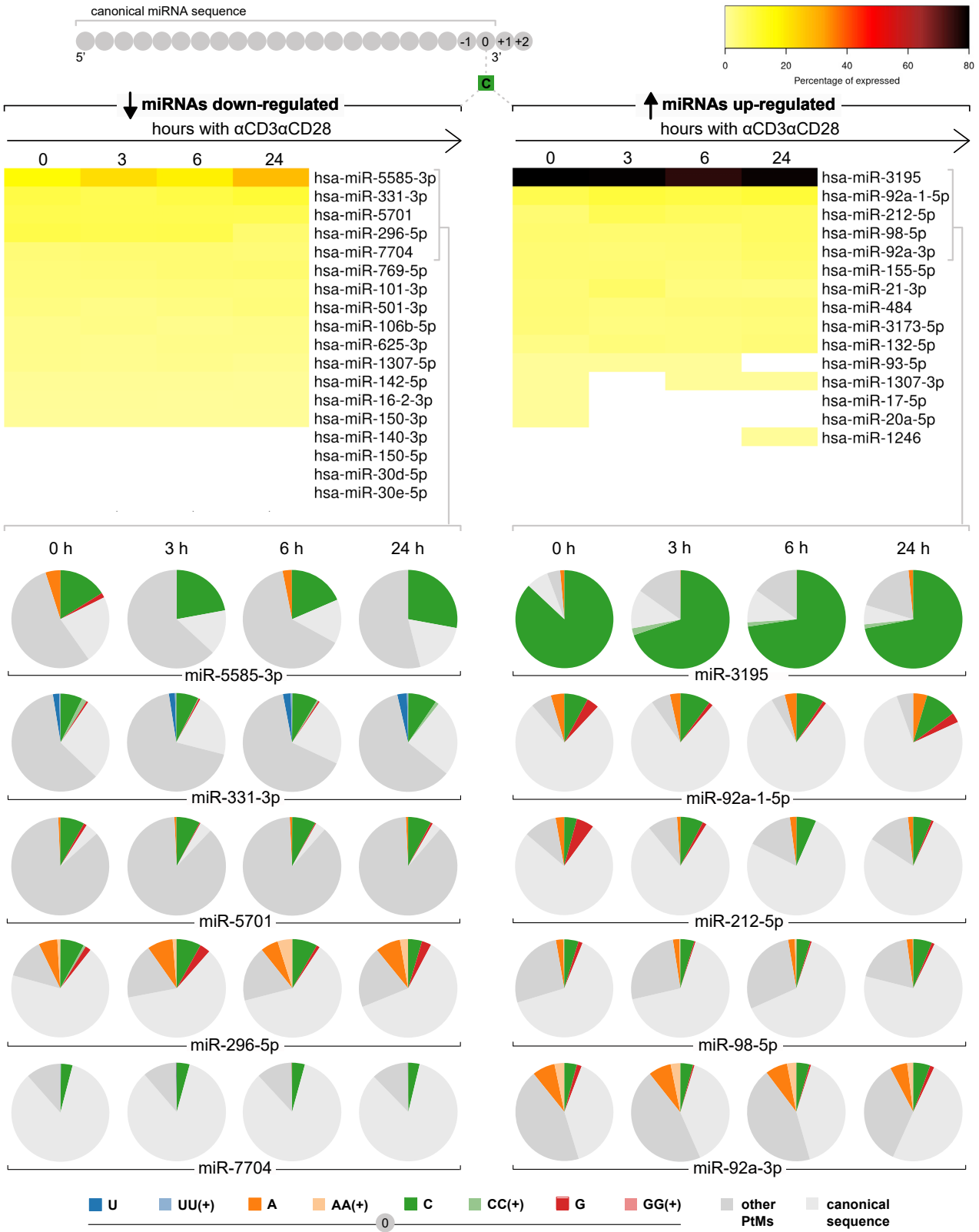
canonical miRNA sequence
5'
-1 0 +1 +2
3'
C
0 20 40 60 80
Percentage of expressed
miRNAs down-regulated
hours with αCD3αCD28
0 3 6 24
hsa-miR-5585-3p
hsa-miR-331-3p
hsa-miR-5701
hsa-miR-296-5p
hsa-miR-7704
hsa-miR-769-5p
hsa-miR-101-3p
hsa-miR-501-3p
hsa-miR-106b-5p
hsa-miR-625-3p
hsa-miR-1307-5p
hsa-miR-142-5p
hsa-miR-16-2-3p
hsa-miR-150-3p
hsa-miR-140-3p
hsa-miR-150-5p
hsa-miR-30d-5p
hsa-miR-30e-5p
miRNAs up-regulated
hours with αCD3αCD28
0 3 6 24
hsa-miR-3195
hsa-miR-92a-1-5p
hsa-miR-212-5p
hsa-miR-98-5p
hsa-miR-92a-3p
hsa-miR-155-5p
hsa-miR-21-3p
hsa-miR-484
hsa-miR-3173-5p
hsa-miR-132-5p
hsa-miR-93-5p
hsa-miR-1307-3p
hsa-miR-17-5p
hsa-miR-20a-5p
hsa-miR-1246
0 h 3 h 6 h 24 h
miR-5585-3p
miR-3195
miR-331-3p
miR-92a-1-5p
miR-5701
miR-212-5p
miR-296-5p
miR-98-5p
miR-7704
miR-92a-3p
U
UU(+)
A
AA(+)
C
CC(+)
G
GG(+)
other PtMs
canonical sequence
0

Figure 7. MiRNAs with significant cytosylation at position 0 (αCD3αCD28)

Heatmaps include upregulated (right) and downregulated (left) miRNAs with significant cytosylation at position 0, detected in αCD3αCD28 stimulation. Reads with cytosine at position 1 are normalized to total reads, in order to visualize the frequency of cytosylation for each miRNA. Pie charts are included below for the 5 miRNAs most adenylated within each group. These graphs show in color the percentage of reads with specific modifications at position 0, while reads with modifications at other positions and unmodified reads are depicted in gray.

8A–8D]. Early upregulation of Eri1 and Dis3L2 could be driving global miRNA downregulation upon T cell activation. The overexpression of TUT4 and TUT7 could be indicating a higher uridylation activity, which could mark miRNA for degradation by Eri1 and Dis3l2.

DISCUSSION

This study aimed to reveal the landscape of PtMs that could control miRNA levels during CD4 T cell activation by antigen T cell receptor and co-receptor (with αCD3αCD28) and by IFN I. We used NGS, since this technique allows the detection of isomiRs variants, offering also for the first time an unbiased exploration of miRNA differential expression at early time points of T cell activation.

Notably, many miRNAs not previously linked with T cell stimulation were significantly down- or upregulated in response to αCD3αCD28. Our repertoire is also consistent with certain miRNAs (e.g. 150-5p, 223-3p, miR-155-5p, miR-17-5p, miR-18a-5p, and miR-4521) previously related with T cell activation in studies performed with arrays, RT-qPCR and Northern Blot (Rodríguez-Galán et al., 2018; Diener et al., 2020), which strengthen our miRNA-seq data. Additionally, we have confirmed our sequencing data through qPCR, including miR-1246 and miR-222-5p ($p = 0.08$) upregulation, and miR-23a-5p and miR-27a-5p downregulation. MiR-1246, miR-23a-5p and miR-27a-5p differential expression was also validated in IFN I stimulation. To our knowledge, no other study has evaluated miRNA changes in human primary T cells stimulated with type I IFN. A recent report reviewed data available on IFN I regulated microRNAs, mainly in the liver cell line Huh7 and human glioma (Forster et al., 2015). Of the 36 miRNAs identified, 7 were described in two or more studies, indicating certain overlapping but also a great diversity across cell types regarding their response to IFN I (Forster et al., 2015). In fact, only one of these 36 miRNAs (miR-212) has been found as differentially expressed in our samples. Two prior studies had assessed immune cells: PBMCs and NK cells. MiRNAs involved in the anti-viral response against Hepatitis C virus (miR-1, miR-30, miR-128, miR-196, and miR-296) were induced in peripheral blood mononuclear cells (PBMCs) upon IFN-α treatment (Scagnolari et al., 2010). In human NK Cells, miRNA-30e and miRNA-378 were downregulated by IFN I (Wang et al., 2012). Our study provides a dataset of IFN I regulated miRNAs in human primary CD4 T cells, which comprises 24 miRNAs that are upregulated and 33 that are downregulated. Of the 57 genes modulated by IFN-I, 37 are also regulated by αCD3αCD28 stimulation.

IPA assessment of IFN-I and αCD3αCD28 regulated miRNAs indicates their involvement in cellular development, growth, proliferation and movement. These processes are indeed essential for activated T cells to perform their function, which includes their differentiation to effector and/or memory phenotypes to combat infection short- and long-term, respectively. In this regard, activated T cells undergo intense cellular reprogramming with an increase in mRNA and protein expression. Accordingly, activated T cells would need to control inhibitory safeguards that prevent abnormal activation that could produce autoimmunity. MiRNA regulation may act as a negative regulator of gene expression, which would need to be withdrawn, at least partially. Several studies support this hypothesis. For instance, mRNAs undergo 3′ UTR shortening upon T lymphocyte activation, thereby reducing the pool of potential target sites for miRNA binding (Sandberg et al., 2008). Moreover, T cell activation promotes a rapid global miRNA downregulation and degradation of Argonaute proteins, which are key effectors of the RISC complex (Bronevetsky et al., 2013). We hypothesize that an active mechanism of miRNA degradation underlies the intense miRNA downregulation observed only a few hours after T cell activation. For this reason, we evaluated the expression of Eri1 and Dis3L2. Both exoribonucleases display a clear preference for uridylated RNA substrates (Chang et al., 2013; Hoefig et al., 2013; Ustianenko et al., 2013); also, Eri1-deficient NK cells and T cells showed increased overall miRNAs levels (Thomas et al., 2012). Here we detected a marked upregulation of both enzymes following T cell activation, pointing toward a context of likely RNA degradation. Enzymes such as, TUT4 and TUT7, which are specifically regulated by αCD3αCD28 stimulation, could be uridylating substrates and labeling them for subsequent degradation by Eri1 or Dis3l2. Interestingly, TUT4 upregulation was not maintained in our samples after 24 hr indicating a potential specific time frame of action for this enzyme.

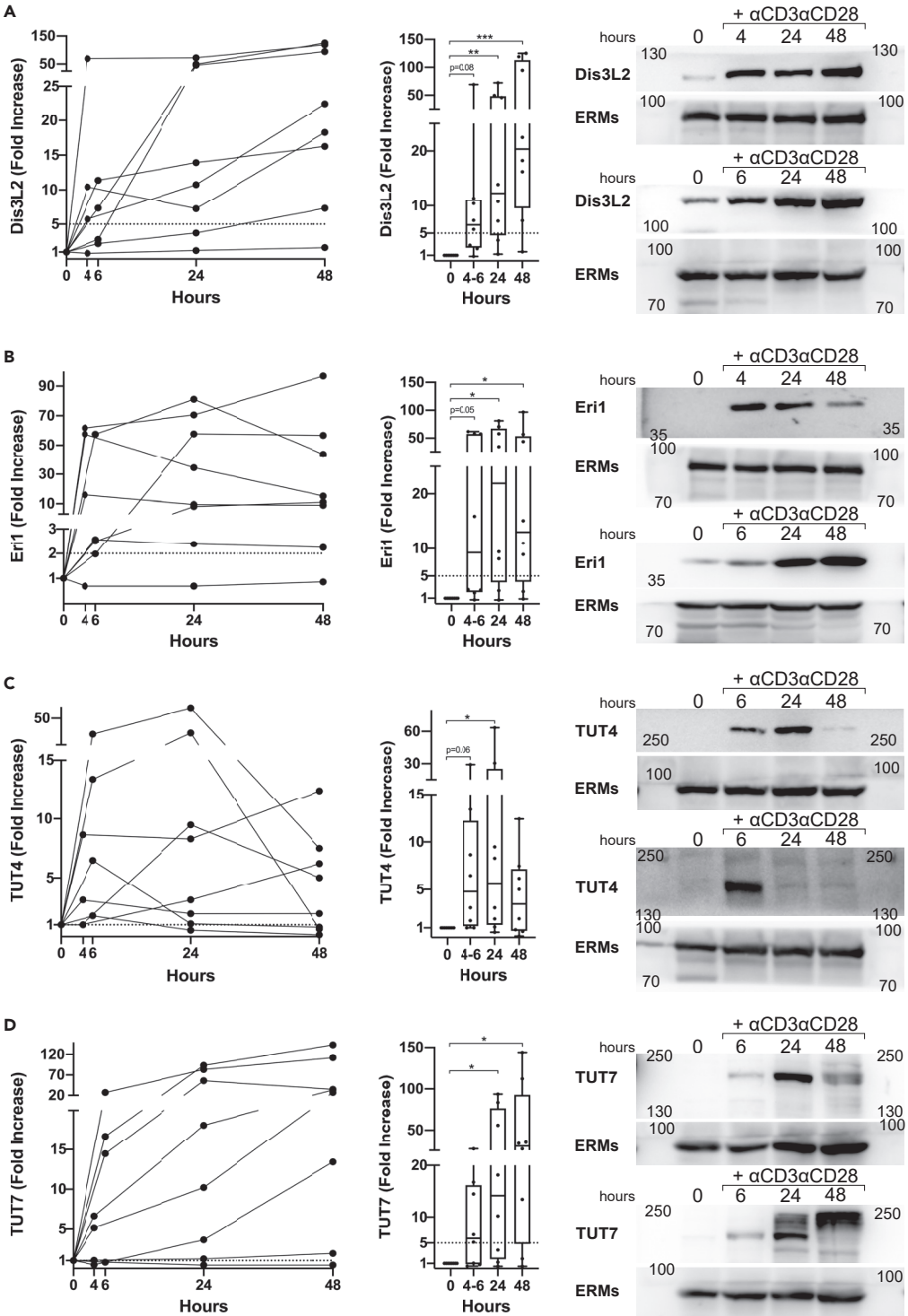

Figure 8. Expression of uridylated RNA degrading enzymes (Dis3L2 and Eri1) and terminal uridyl transferases (TUT4 y TUT7) upon CD4+ T cell activation

Western blot analysis of protein expression in human primary CD4+ T cells from 8 donors stimulated with αCD3αCD28, assessing Dis3L2 (A), Eri1 (B), TUT4 (C) and TUT7 (D). Fold increase compared to non-stimulation was represented for each donor, to observe individual expression evolution upon activation (left panel), and using group median and interquartile range with whiskers ranging from minimum to maximum values (middle panel). Right panels include two examples of different donors for each protein to highlight inter-donor variability in upregulation kinetics. Band intensities were

Figure 8. *Continued*
normalized to ERMs values and relativized to unstimulated conditions. Statistical analysis: Kruskal-Wallis test, Dunn's multiple comparisons test [* p value <0.05, ** p value<0.01, *** p value<0.001; 0.05<p value<0.1: indicated with numbers]. In panel C, TUT4 was separated under two different acrylamide gel concentrations.

Nevertheless, T cells still require certain miRNAs to remain stable even in generally degradative conditions. PtMs could control miRNA stability, promoting degradation but also protecting specific miRNAs. The global PtMs profile of our samples reveals that modification processes were focused on the 3′ end of most miRNAs. A series of upregulated miRNAs, particularly in αCD3αCD28, show a higher degree of adenylation, which could be related with miRNA stability in the context of T cells. Interestingly, the most adenylated miRNA (with up to a 42% of reads adenylated at position 1) is miR-92a-3p which is precisely the upregulated miRNA with higher expression in both studied activation conditions. Other miRNAs highly adenylated such as miR-17-5p, miR-93-5p, miR-20a-5p, and miR-378a-3p are also among those αCD3αCD28-upregulated miRNAs expressed with greater abundance.

While uridylation and adenylation have been the best characterized 3′ end modifications described across animal miRNAs (Burroughs et al., 2010; Chiang et al., 2010; Landgraf et al., 2007; Muller et al., 2014; Wyman et al., 2011), cytosylation was also significantly represented in our samples. Cytosine was specifically found at position 0 (3′ end nucleotide). Although most studies evaluating PtMs have found guanosine and cytosine additions to be barely represented, mono-addition of cytosine was the second most abundant 3′ modification after mono-uridylation, in mouse primordial germ cells and gonadal somatic cells at various embryonic stages (Darnell et al., 2018). The presence of "non-templated cytosylation" has been described in Arabidopsis, which prompted the hypothesis of the existence of a nucleotidyl transferase with a preference for cytosine as substrate (Chou et al., 2015). Cytosine additions could be relevant for miRNA modulation in very specific developmental or differentiation stages.

Consistent with previous studies from our laboratory, which had indicated that uridylation is a miRNA degradation signal in T cells (Gutiérrez-Vázquez et al., 2017), higher levels of U additions were found in αCD3αCD28 downregulated miRNAs. A similar pattern can be observed in IFN I stimulation, although differences are milder, which may be due to a less dynamic miRNA environment; since the number of differentially expressed miRNAs was roughly half of those quantified in cells treated with αCD3αCD28.

In summary, this study offers a data set of differentially regulated miRNAs in early time points of human primary CD4+ T cell activation and the kinetics of their PtMs. Our data also indicate that the RNA degrading enzymes Eri1 and Dis3L2 are upregulated upon activation, which could be part of an active mechanism of miRNA degradation guided by uridylation. Indeed, higher uridylation was found in downregulated miRNAs. Upregulated miRNAs, which manage to multiply their levels in this adverse environment, point toward 3′ adenine addition as a potential protective signal.

Limitations of the study

The present study is technically limited by the lack of solid tools for the study of single miRNA modifications beyond NGS. In addition, our data will need to be further completed with a better understanding of ribonucleases and RNA partners behind the modification landscape observed here. This study will be highly complex due to the numerous potential players and the difficulty to identify proteins with enzymatic activities barely described so far, such as cytosine addition. Therefore, we prefer to make this earlier approach available now to the scientific community, being aware that there is still much to learn on the field.

STAR★METHODS

Detailed methods are provided in the online version of this paper and include the following:

- KEY RESOURCES TABLE
- RESOURCE AVAILABILITY
  - Lead contact
  - Materials availability
  - Data and code availability
- EXPERIMENTAL MODEL AND SUBJECT DETAILS

SUPPLEMENTAL INFORMATION

Supplemental information can be found online at https://doi.org/10.1016/j.isci.2021.102530.

ACKNOWLEDGMENTS

We thank Miguel Vicente-Manzanares and Simon Bartlett for help with English. We also thank the CNIC Genomics and Bioinformatics Units for technical support.

This work was supported by grants SAF2017-82886-R from the Spanish Ministry of Economy and Competitiveness (MINECO), grant S2017/BMD-3671-INFLAMUNE-CM from the Comunidad de Madrid, a grant from the Ramón Areces Foundation "Ciencias de la Vida y la Salud" (XIX Concurso-2018) and a grant from Ayudas Fundación BBVA an Equipos de Investigación Científica (BIOMEDICINA-2018) and ""la Caixa"" Banking Foundation (HR17-00016). BIOIMID (PIE13/041) from Instituto de Salud Carlos III, CIBER Cardiovascular (CB16/11/00272, Fondo de Investigación Sanitaria del Instituto de Salud Carlos III and co-funding by Fondo Europeo de Desarrollo Regional FEDER). The Centro Nacional de Investigaciones Cardiovasculares (CNIC, Spain) is supported by the Ministerio de Economía y Competitividad-Spain and the Pro-CNIC Foundation.

A.R.G., S.G.D., and I.F.D. were supported by the FPU program (Spanish Ministry of Education).

AUTHOR CONTRIBUTIONS

A.R.G. and F.S.M. conceived the study. Experiments were performed by A.R.G., S.G.D., and I.F.D. L.F.M. provided miRNA expertise advice and discussion. M.J.G. and F.S.C. performed the differential expression and PtMs analysis of the miRNA-seq data. A.R.G. analyzed results, made the figures and wrote the manuscript, with input from the rest of authors. F.S.M. supervised and revised all the work.

DECLARATION OF INTERESTS

The authors declare no competing interests.

Received: October 14, 2020
Revised: April 6, 2021
Accepted: May 10, 2021
Published: June 25, 2021

REFERENCES

Bazak, L., Haviv, A., Barak, M., Jacob-Hirsch, J., Deng, P., Zhang, R., Isaacs, F.J., Rechavi, G., Li, J.B., Eisenberg, E., et al. (2014). A-to-I RNA editing occurs at over a hundred million genomic sites, located in a majority of human genes. Genome Res. *24*, 365–376.

Blanc, V., and Davidson, N.O. (2010). APOBEC-1-mediated RNA editing. Wiley Interdiscip. Rev. Syst. Biol. Med. *2*, 594–602.

Boele, J., Persson, H., Shin, J.W., Ishizu, Y., Newie, I.S., Søkilde, R., Hawkins, S.M., Coarfa, C., Ikeda, K., Takayama, K.I., et al. (2014). PAPD5-mediated 3′ adenylation and subsequent degradation of miR-21 is disrupted in proliferative disease. Proc. Natl. Acad. Sci. U S A *111*, 11467–11472.

Bronevetsky, Y., Villarino, A.V., Eisley, C.J., Barbeau, R., Barczak, A.J., Heinz, G.A., Kremmer, E., Heissmeyer, V., McManus, M.T., Erle, D.J., et al. (2013). T cell activation induces proteasomal degradation of Argonaute and rapid remodeling of the microRNA repertoire. J. Exp. Med. *210*, 417–432.

Burroughs, A.M., Ando, Y., de Hoon, M.J.L., Tomaru, Y., Nishibu, T., Ukekawa, R., Funakoshi, T., Kurokawa, T., Suzuki, H., Hayashizaki, Y., et al. (2010). A comprehensive survey of 3′ animal miRNA modification events and a possible role for 3′ adenylation in modulating miRNA targeting effectiveness. Genome Res. *20*, 1398–1410.

Büssing, I., Slack, F.J., and Großhans, H. (2008). let-7 microRNAs in development, stem cells and cancer. Trends Mol. Med. *14*, 400–409.

Chang, H.-M., Triboulet, R., Thornton, J.E., and Gregory, R.I. (2013). A role for the Perlman syndrome exonuclease Dis3l2 in the Lin28-let-7 pathway. Nature *497*, 244–248.

Chiang, H.R., Schoenfeld, L.W., Ruby, J.G., Auyeung, V.C., Spies, N., Baek, D., Johnston, W.K., Russ, C., Luo, S., Babiarz, J.E., et al. (2010). Mammalian microRNAs: experimental evaluation of novel and previously annotated genes. Genes Dev. *24*, 992–1009.

Chou, M.-T., Han, B.W., Hsiao, C.-P., Zamore, P.D., Weng, Z., and Hung, J.-H. (2015). Tailor: a

computational framework for detecting non-templated tailing of small silencing RNAs. Nucleic Acids Res. *43*, 109.

D'Ambrogio, A., Gu, W., Udagawa, T., Mello, C.C., and Richter, J.D. (2012). Specific miRNA stabilization by Gld2-catalyzed monoadenylation. Cell Rep. *2*, 1537–1545.

Darnell, R.B., Ke, S., and Darnell, J.E. (2018). Protein–RNA interactions: structural characteristics and hotspot amino acids. Rna *24*, 1457–1465.

Diener, C., Hart, M., Kehl, T., Rheinheimer, S., Ludwig, N., Krammes, L., Pawusch, S., Lenhof, K., Tänzer, T., Schub, D., et al. (2020). Quantitative and time-resolved miRNA pattern of early human T cell activation. Nucleic Acids Res. *48*, 10164–10183.

Ebhardt, H.A., Tsang, H.H., Dai, D.C., Liu, Y., Bostan, B., and Fahlman, R.P. (2009). Meta-analysis of small RNA-sequencing errors reveals ubiquitous post-transcriptional RNA modifications. Nucleic Acids Res. *37*, 2461–2470.

Fan, Y., and Xia, J. (2018). miRNet—functional analysis and visual exploration of miRNA–target interactions in a network context. In Methods in Molecular Biology (Humana Press Inc.), pp. 215–233.

Forster, S.C., Tate, M.D., and Hertzog, P.J. (2015). MicroRNA as type I interferon-regulated transcripts and modulators of the innate immune response. Front. Immunol. *6*, 1.

Gebert, L.F.R., and MacRae, I.J. (2019). Regulation of microRNA function in animals. Nat. Rev. Mol. Cell Biol. *20*, 21–37.

Gracias, D.T., and Katsikis, P.D. (2011). MicroRNAs: key components of immune regulation. In Advances in Experimental Medicine and Biology (Adv Exp Med Biol), pp. 15–26.

Grigoryev, Y.A., Kurian, S.M., Hart, T., Nakorchevsky, A.A., Chen, C., Campbell, D., Head, S.R., Yates, J.R., and Salomon, D.R. (2011). MicroRNA regulation of molecular networks mapped by global microRNA, mRNA, and protein expression in activated T lymphocytes. J. Immunol. *187*, 2233–2243.

Gu, S., Jin, L., Zhang, Y., Huang, Y., Zhang, F., Valdmanis, P.N., and Kay, M.A. (2012). The loop position of shRNAs and pre-miRNAs is critical for the accuracy of dicer processing in vivo. Cell *151*, 900–911.

Gutiérrez-Vázquez, C., Enright, A.J., Rodríguez-Galán, A., Pérez-García, A., Collier, P., Jones, M.R., Benes, V., Mizgerd, J.P., Mittelbrunn, M., Ramiro, A.R., et al. (2017). 3′ Uridylation controls mature microRNA turnover during CD4 T-cell activation. RNA *23*, 882–891.

Heo, I., Joo, C., Cho, J., Ha, M., Han, J., and Kim, V.N. (2008). Lin28 mediates the terminal uridylation of let-7 precursor MicroRNA. Mol. Cell *32*, 276–284.

Heo, I., Joo, C., Kim, Y.-K., Ha, M., Yoon, M.-J., Cho, J., Yeom, K.-H., Han, J., and Kim, V.N. (2009). TUT4 in concert with Lin28 suppresses microRNA biogenesis through pre-microRNA uridylation. Cell *138*, 696–708.

Heo, I., Ha, M., Lim, J., Yoon, M.J., Park, J.E., Kwon, S.C., Chang, H., and Kim, V.N. (2012). Mono-uridylation of pre-microRNA as a key step in the biogenesis of group II let-7 microRNAs. Cell *151*, 521–532.

Hoefig, K.P., Rath, N., Heinz, G.A., Wolf, C., Dameris, J., Schepers, A., Kremmer, E., Ansel, K.M., and Heissmeyer, V. (2013). Eri1 degrades the stem-loop of oligouridylated histone mRNAs to induce replication-dependent decay. Nat. Struct. Mol. Biol. *20*, 73–81.

Jindra, P.T., Bagley, J., Godwin, J.G., and Iacomini, J. (2010). Costimulation-Dependent expression of MicroRNA-214 increases the ability of T cells to proliferate by targeting Pten. J. Immunol. *185*, 990–997.

Jones, M.R., Quinton, L.J., Blahna, M.T., Neilson, J.R., Fu, S., Ivanov, A.R., Wolf, D.A., and Mizgerd, J.P. (2009). Zcchc11-dependent uridylation of microRNA directs cytokine expression. Nat. Cell Biol. *11*, 1157–1163.

Katoh, T., Sakaguchi, Y., Miyauchi, K., Suzuki, T., Suzuki, T., Kashiwabara, S.I., and Baba, T. (2009). Selective stabilization of mammalian microRNAs by 3′ adenylation mediated by the cytoplasmic poly(A) polymerase GLD-2. Genes Dev. *23*, 433–438.

Kim, B., Jeong, K., and Kim, V.N. (2017). Genome-wide mapping of DROSHA cleavage sites on primary MicroRNAs and noncanonical substrates. Mol. Cell *66*, 258–269.e5.

Kwon, S.C., Baek, S.C., Choi, Y.G., Yang, J., Lee, Y.S., Woo, J.S., and Kim, V.N. (2019). Molecular basis for the single-nucleotide precision of primary microRNA processing. Mol. Cell *73*, 505–518.e5.

Landgraf, P., Rusu, M., Sheridan, R., Sewer, A., Iovino, N., Aravin, A., Pfeffer, S., Rice, A., Kamphorst, A.O., Landthaler, M., et al. (2007). A mammalian microRNA expression atlas based on small RNA library sequencing. Cell *129*, 1401–1414.

Lee, L.W., Zhang, S., Etheridge, A., Ma, L., Martin, D., Galas, D., and Wang, K. (2010). Complexity of the microRNA repertoire revealed by next-generation sequencing. RNA *16*, 2170–2180.

Li, B., and Dewey, C.N. (2011). RSEM: accurate transcript quantification from RNA-Seq data with or without a reference genome. BMC Bioinformatics *12*, 323.

Li, L., Song, Y., Shi, X., Liu, J., Xiong, S., Chen, W., Fu, Q., Huang, Z., Gu, N., and Zhang, R. (2018). The landscape of miRNA editing in animals and its impact on miRNA biogenesis and targeting. Genome Res. *28*, 132–143.

Lindsay, M.A. (2008). microRNAs and the immune response. Trends Immunol. *29*, 343–351.

Martin, M. (2011). Cutadapt removes adapter sequences from high-throughput sequencing reads. EMBnet. J. *17*, 10–12.

Mehta, A., and Baltimore, D. (2016). MicroRNAs as regulatory elements in immune system logic. Nat. Rev. Immunol. *16*, 279–294.

Muller, H., Marzi, M.J., and Nicassio, F. (2014). IsomiRage: from functional classification to differential expression of miRNA isoforms. Front. Bioeng. Biotechnol. *2*, 38.

Neilsen, C.T., Goodall, G.J., and Bracken, C.P. (2012). IsomiRs–the overlooked repertoire in the dynamic microRNAome. Trends Genet. *28*, 544–549.

Nishikura, K. (2016). A-to-I editing of coding and non-coding RNAs by ADARs. Nat. Rev. Mol. Cell Biol. *17*, 83–96.

Podshivalova, K., and Salomon, D.R. (2013). MicroRNA regulation of T-lymphocyte immunity: modulation of molecular networks responsible for T-cell activation, differentiation, and development. Crit. Rev. Immunol. *33*, 435–476.

Ritchie, M.E., Phipson, B., Wu, D., Hu, Y., Law, C.W., Shi, W., and Smyth, G.K. (2015). Limma powers differential expression analyses for RNA-sequencing and microarray studies. Nucleic Acids Res. *43*, e47.

Rodríguez-Galán, A., Fernández-Messina, L., and Sánchez-Madrid, F. (2018). Control of immunoregulatory molecules by miRNAs in T cell activation. Front. Immunol. *9*, 1–10.

Rosenberg, B.R., Hamilton, C.E., Mwangi, M.M., Dewell, S., Papavasiliou, F.N., Struct, N., and Biol, M. (2011). Transcriptome-wide sequencing reveals numerous APOBEC1 mRNA editing targets in transcript 3′ UTRs HHS Public Access Author manuscript. Nat. Struct. Mol. Biol. *18*, 230–236.

Sandberg, R., Neilson, J.R., Sarma, A., Sharp, P.A., and Burge, C.B. (2008). Proliferating cells express mRNAs with shortened 3′ untranslated regions and fewer MicroRNA target sites. Science *320*, 1643–1647.

Scagnolari, C., Zingariello, P., Vecchiet, J., Selvaggi, C., Racciatti, D., Taliani, G., Riva, E., Pizzigallo, E., and Antonelli, G. (2010). Differential expression of interferon-induced microRNAs in patients with chronic hepatitis C virus infection treated with pegylated interferon alpha. Virol. J. *7*, 311.

Sousa, I.G., do Almo, M.M., Simi, K.C.R., Bezerra, M.A.G., Andrade, R.V., Maranhão, A.Q., and Brigido, M.M. (2017). MicroRNA expression profiles in human CD3+T cells following stimulation with anti-human CD3 antibodies. BMC Res. Notes *10*, 124.

de Sousa, M.C., Gjorgjieva, M., Dolicka, D., Sobolewski, C., and Foti, M. (2019). Deciphering miRNAs' action through miRNA editing. Int. J. Mol. Sci. *20*, 6249.

Starega-Roslan, J., Krol, J., Koscianska, E., Kozlowski, P., Szlachcic, W.J., Sobczak, K., and Krzyzosiak, W.J. (2011). Structural basis of microRNA length variety. Nucleic Acids Res. *39*, 257–268.

Sturn, A., Quackenbush, J., and Trajanoski, Z. (2002). Genesis: cluster analysis of microarray data. Bioinformatics *18*, 207–208.

Tan, M.H., Li, Q., Shanmugam, R., Piskol, R., Kohler, J., Young, A.N., Liu, K.I., Zhang, R., Ramaswami, G., Ariyoshi, K., et al. (2017). Dynamic landscape and regulation of RNA editing in mammals. Nature *550*, 249–254.

Teteloshvili, N., Smigielska-Czepiel, K., Kroesen, B.-J., Brouwer, E., Kluiver, J., Boots, A., and van den Berg, A. (2015). T-cell activation induces dynamic changes in miRNA expression patterns in CD4 and CD8 T-cell subsets. MicroRNA *4*, 117–122.

Thomas, M.F., Abdul-Wajid, S., Panduro, M., Babiarz, J.E., Rajaram, M., Woodruff, P., Lanier, L.L., Heissmeyer, V., and Ansel, K.M. (2012). Eri1 regulates microRNA homeostasis and mouse lymphocyte development and antiviral function. Blood *120*, 130–142.

Thornton, J.E., Chang, H.M., Piskounova, E., and Gregory, R.I. (2012). Lin28-mediated control of let-7 microRNA expression by alternative TUTases Zcchc11 (TUT4) and Zcchc6 (TUT7). RNA *18*, 1875–1885.

Ustianenko, D., Hrossova, D., Potesil, D., Chalupnikova, K., Hrazdilova, K., Pachernik, J., Cetkovska, K., Uldrijan, S., Zdrahal, Z., and Vanacova, S. (2013). Mammalian DIS3L2 exoribonuclease targets the uridylated precursors of let-7 miRNAs. RNA *19*, 1632–1638.

Vitsios, D.M., and Enright, A.J. (2015). Chimira: analysis of small RNA sequencing data and microRNA modifications. Bioinformatics *31*, 3365–3367.

Wang, Y., and Liang, H. (2018). When MicroRNAs meet RNA editing in cancer: a nucleotide change can make a difference. BioEssays *40*. https://doi.org/10.1002/bies.201700188.

Wang, P., Gu, Y., Zhang, Q., Han, Y., Hou, J., Lin, L., Wu, C., Bao, Y., Su, X., Jiang, M., et al. (2012). Identification of Resting and Type I IFN-Activated Human NK Cell miRNomes Reveals MicroRNA-378 and MicroRNA-30e as Negative Regulators of NK Cell Cytotoxicity. J. Immunol. *189*, 211–221.

Warkocki, Z., Liudkovska, V., Gewartowska, O., Mroczek, S., and Dziembowski, A. (2018). Terminal nucleotidyl transferases (TENTs) in mammalian RNA metabolism. Philos. Trans. R. Soc. B Biol. Sci. *373*, 20180162.

Wu, H., Neilson, J.R., Kumar, P., Manocha, M., Shankar, P., Sharp, P.A., and Manjunath, N. (2007). miRNA profiling of naïve, effector and memory CD8 T cells. PLoS One *2*, e1020.

Wu, H., Ye, C., Ramirez, D., and Manjunath, N. (2009). Alternative processing of primary microRNA transcripts by Drosha generates 5′ end variation of mature microRNA. PLoS One *4*, e7566.

Wyman, S.K., Knouf, E.C., Parkin, R.K., Fritz, B.R., Lin, D.W., Dennis, L.M., Krouse, M.A., Webster, P.J., and Tewari, M. (2011). Post-transcriptional generation of miRNA variants by multiple nucleotidyl transferases contributes to miRNA transcriptome complexity. Genome Res. *21*, 1450–1461.

Yang, Q., Lin, J., Liu, M., Li, R., Tian, B., Zhang, X., Xu, B., Liu, M., Zhang, X., Li, Y., et al. (2016). Highly sensitive sequencing reveals dynamic modifications and activities of small RNAs in mouse oocytes and early embryos. Sci. Adv. *2*, e1501482.

Yang, W., Chendrimada, T.P., Wang, Q., Higuchi, M., Seeburg, P.H., Shiekhattar, R., and Nishikura, K. (2006). Modulation of microRNA processing and expression through RNA editing by ADAR deaminases. Nat. Struct. Mol. Biol. *13*, 13–21.

Zhou, H., Arcila, M.L., Li, Z., Lee, E.J., Henzler, C., Liu, J., Rana, T.M., and Kosik, K.S. (2012). Deep annotation of mouse iso-miR and iso-moR variation. Nucleic Acids Res. *40*, 5864–5875.

Zhu, L., Kandasamy, S.K., and Fukunaga, R. (2018). Dicer partner protein tunes the length of miRNAs using base-mismatch in the pre-miRNA stem. Nucleic Acids Res. *46*, 3726–3741.

STAR★METHODS

KEY RESOURCES TABLE

REAGENT or RESOURCE	SOURCE	IDENTIFIER
Antibodies		
anti-Dis3L2	Nobus biologicals	Cat# NBP1-84740
anti-Eri1/THEX1	Cell Signaling	Cat#4049
anti-TUT4/ZCCHC11	Pro Sci incorporated	Cat#46-610
anti-TUT7/ZCCHC6	Proteintech	Cat#25196-1-AP
anti-ezrin/radixin/moesin (ERMs) (90/3)	provided by Heinz Furthmayr, Stanford University, CA	N/A
goat anti-rabbit	ThermoFisher Scientific	Cat#31460
rabbit anti-goat	ThermoFisher Scientific	Cat#31402
Biological samples		
Buffy coats	Centro de Transfusión (Comunidad de Madrid, Spain)	N/A
Chemicals, peptides, and recombinant proteins		
Biocoll Separating Solution	Biochrom	Cat# L6115
ImmunoCult™ Human CD3/CD28 T Cell Activator	STEMCELL Technologies	Cat#10971
Human IFN Alpha Hybrid (Universal Type I IFN)	PBL ASSAY SCIENCE	Cat#11200-1
QIAzol Lysis Reagent	Qiagen	Cat#, 79306
Critical commercial assays		
Human Resting CD4+ T cell Isolation Kit	STEMCELL Technologies	Cat#17962
EasySep Human CD4+ T Cell Isolation Kit	STEMCELL Technologies	Cat#17952
miRNeasy Mini Kit	Qiagen	Cat#217004
NEBNext Multiplex SmallRNA Library Prep Set for Illumina	New England Biolabs	Cat#E7580L
miRCURY LNA RT Kit	Qiagen	Cat#339340
miRCURY LNA SYBER Green PCR Kit	Qiagen	Cat#339347
miRCURY LNA miRNA PCR Assay(hsa-miR-1246, hsa-miR-222-5p, hsa-miR-23a-5p, hsa-miR-27a-5p, SNORD44(hsa) and SNORD48(hsa))	Qiagen	Cat#339306
Deposited data		
Raw and processed data	This paper	GEO: GSE156287
Alignments IFN I	This paper	https://genome.ucsc.edu/s/mjgommo/CD4T_IFN_I
Alignments aCD3aCD28	This paper	https://genome.ucsc.edu/s/mjgommo/CD4T_aCD3aCD28
In-house script (CHIMProcessor.R)	This paper	https://github.com/mjgommo/CD4T_miRNA_MOD
Software and algorithms		
FastQC	Babraham Bioinformatics	http://www.bioinformatics.babraham.ac.uk/projects/fastqc/
Cutadapt	Martin (2011)	http://code.google.com/p/cutadapt/
RSEM	Li and Dewey (2011)	http://deweylab.biostat.wisc.edu/rsem
Bioconductor package Limma	Ritchie et al. (2015)	https://bioconductor.org/packages/release/bioc/html/limma.html
Genesis	Sturn et al. (2002)	http://genome.tugraz.at
Chimira	Vitsios and Enright (2015)	http://wwwdev.ebi.ac.uk/enright-dev/chimira/

(*Continued on next page*)

Continued

REAGENT or RESOURCE	SOURCE	IDENTIFIER
Ingenuity Pathway Analysis	Qiagen	Content version: 49932394
MiRNet	Fan and Xia (2018)	www.mirnet.ca
Biogazelle	QbasePlus	https://www.qbaseplus.com
Image Studio Lite	LI-COR Biosciences	https://www.licor.com/bio/image-studio-lite/download

RESOURCE AVAILABILITY

Lead contact

Further information and requests for resources and reagents should be directed to and will be fulfilled by the Lead Contact, Francisco Sánchez-Madrid (fsmadrid@salud.madrid.org).

Materials availability

This study did not generate new unique reagents.

Data and code availability

GEO submission. All raw and processed sequencing data generated in this study have been submitted to the NCBI Gene Expression Omnibus (GEO; https://www.ncbi.nlm.nih.gov/geo/) under accession number GSE156287.

UCSC genome browser sessions. Alignments are accessible at the following UCSC Genome Browser session:

* https://genome.ucsc.edu/s/mjgommo/CD4T_IFN_I
* https://genome.ucsc.edu/s/mjgommo/CD4T_aCD3aCD28

Each session has been configured to allow the visualization of 13 custom tracks, which consist in:

- miRBase_mature track: representing the coordinates of all mature miRNAs described in miRBase, release 22.
-12 BAM alignment tracks, corresponding to three replicate samples for the control condition (0h) and each of the time points (3h, 6h, 24h) for IFN I or αCD3αCD28 treatment.

MiRNA detection and quantification have been performed in this study by aligning NGS processed reads against a transcriptomic reference consisting in all mature miRNA sequences described in miRBAse, release 22, for Homo sapiens. To produce genomic alignments that were fully congruent with those generated for quantification, BAM alignments displayed in the UCSC tracks have been generated with RSEM using a genomic reference constructed with the mature miRNA coordinates described in miRBase, release 22, exclusively. For this reason, coverage is expected only at the intervals corresponding to regions that code for mature miRNAs. MIMAT IDs are used to identify such intervals because they are guaranteed to be unique (locus specific). Visualization of the tracks may require reloading the page, because of timeout issues.

In-house scripts. Chimira results describing miRNA modifications consist in a separate table for each sample. A specialized, in-house R script (CHIMProcessor.R) was developed to process the collection of output files, as well as several other auxiliary files, in order to normalize modification frequencies by library size, merge frequency information from replicate samples, filter data using various parameters and generate combined tables and preliminary plots. The script is available from GitHub, at:

* https://github.com/mjgommo/CD4T_miRNA_MOD

EXPERIMENTAL MODEL AND SUBJECT DETAILS

Human primary cells used in this study were isolated from healthy donor buffy coats. Donor age and sex were not disclosed by the medical center providing the samples.

These studies were performed according to the principles of the Declaration of Helsinki and approved by the local Ethics Committee for Basic Research at the Hospital La Princesa (Madrid), informed consent was obtained from all human volunteers.

Cells were cultured at 37°C in RPMI 1640 (Gibco), supplemented with 10% fetal bovine serum (Sigma), 20mM Hepes (Hyclone), 0.3mg/mL L-glutamine (Hyclone), 100 U/mL penicillin (Gibco) and 100 µg/mL streptomycin (Gibco).

METHOD DETAILS

Human primary CD4 T cell culture

Human peripheral blood mononuclear cells (PBMCs) were isolated from buffy coats, obtained from healthy donors, by separation on Biocoll Separating Solution (Biochrom, L6115) according to standard procedures. Non-adherent cells were separated from PBMCs after a 30 min adherence step at 37°C. $CD4^+$ T cells were purified from non-adherent cells using Human Resting CD4+ T cell Isolation Kit (STEMCELL Technologies, 17962). A specific reagent to isolate resting T cells was selected to avoid the presence of pre-activated CD4+ T cells in sequencing samples. In experiments performed to evaluate protein expression, CD4+ T cells were isolated with EasySep Human CD4+ T Cell Isolation Kit (STEMCELL Technologies, 17952).

For T cell stimulation, we treated CD4+ T cells with either αCD3αCD28 (ImmunoCult™ Human CD3/CD28 T Cell Activator; STEMCELL Technologies, 10971) or IFN I (1:1000, Human IFN Alpha Hybrid (Universal Type I IFN); PBL ASSAY SCIENCE, 11200-1).

RNA isolation, library preparation and NGS

Three independent experiments, with resting CD4+ T cells isolated from different healthy donors were performed. Samples were collected at 0h and after αCD3αCD28 or IFN I stimulation during 3h, 6h and 24h. The 21 samples were lysed in QIAzol Lysis Reagent (Qiagen, 79306) and RNA was extracted using the miRNeasy Mini Kit (Qiagen, 217004). In order to reduce phenol-based reagent contaminations, purified RNA samples were precipitated using sodium acetate (3M, 0.1x sample volume) and ethanol (100%,3x sample volume). RNA integrity was evaluated using an Agilent 2100 Bioanalyzer (Eukaryote Total RNA Nano assay).

A total of 200 ng of total RNA were used to generate barcoded miRNA-seq libraries using the NEBNext Multiplex SmallRNA Library Prep Set for Illumina (New England Biolabs). Briefly, 3′ and 5′ SR adapters were first ligated to the RNA sample. Next, reverse transcription followed by PCR amplification was used to enrich cDNA fragments with adapters at both ends. The quantity and quality of the miRNA libraries were determined using the Agilent 2100 Bioanalyzer High Sensitivity DNA chip.

Libraries were sequenced on a HiSeq2500 (Illumina) to generate 60 bases single reads. FastQ files for each sample were obtained using bcltofastQ 2.20 Software software (Illumina). NGS experiments were performed in the Genomics Unit of the CNIC.

miRNA-seq data analysis

Sequencing reads were pre-processed by means of a pipeline that used FastQC (http://www.bioinformatics.babraham.ac.uk/projects/fastqc/) to assess read quality; and Cutadapt (Martin, 2011) to trim sequencing reads, eliminating Illumina adapter remains, and to discard those that were shorter than 15 nt or longer than 35 nt after trimming. Around 80% of the reads from any of the samples were retained. Resulting reads were aligned against a collection of 2657 human, mature miRNA sequences extracted from miRBase (release 22), to obtain expression estimates with RSEM (Li and Dewey, 2011). Percentages of reads participating in at least one reported alignment were around 40%. Expected expression counts were then processed with an analysis pipeline that used Bioconductor package Limma (Ritchie et al., 2015) for normalization (using TMM method) and differential expression testing, taking into account that samples had been obtained in three batches, and considering only 626 miRNA species for which expression was at least 1 count per million (CPM) in 3 samples. Changes in gene expression were

considered significant if associated to Benjamini-Hochberg adjusted p-value < 0.1. Clustering of expression profiles and production of heatmaps were performed with Genesis (Sturn et al., 2002). Epi-transcriptomic modifications were detected with Chimira (Vitsios and Enright, 2015), an online tool that, after alignment of miRNA-seq reads against miRBAse records, identifies mismatched positions to classify them and to quantify multiple types of 3'-modifications (uridylation, for example), as well as 5'-modifications and internal modifications or variations. Count tables produced by Chimira were further processed with ad-hoc produced R-scripts to normalize modification counts by library size and to calculate summary statistics across groups of replicate samples. Analyses were restricted to the collection of 626 miRNA species with detectable expression. Upregulated and downregulated miRNA groups were defined considering any significant differential expression including all possible time point comparisons, not only those performed versus 0h.

Two core analysis were performed by Ingenuity Pathway Analysis (Content version: 49932394 (Release Date: 2019-11-14), one with all miRNAs differentially expressed at least at one time point after stimulation with αCD3αCD28 and a second one with the corresponding IFN-I regulated miRNAs. MiRNA-target networks were built with miRNet loading the highest upregulated and downregulated miRNAs for each treatment (Fan and Xia, 2018). Venn diagrams were elaborated with Venny (https://bioinfogp.cnb.csic.es/tools/venny/index.html).

miRNA qPCR

RNA was retrotranscribed using miRCURY LNA RT Kit (Qiagen, 339340) and qPCR was performed using miRCURY LNA SYBER Green PCR Kit (Qiagen, 339347) in AB7900. Primers for hsa-miR-1246, hsa-miR-222-5p, hsa-miR-23a-5p, hsa-miR-27a-5p, SNORD44 (hsa) and SNORD48 (hsa) were obtained from miRCURY LNA miRNA PCR Assay (Qiagen, 339306). Data was analyzed with Biogazelle QbasePlus software. Expression values were normalized to both RNU44 and RNU48.

IMMUNOBLOTTING

Cell extracts were prepared in lysis buffer (50 mM Tris pH 7.5, 150 mM NaCl, 1%NP-40, 5 mM EDTA, 50mM NaF, 5mM DTT) supplemented with a protease inhibitor cocktail (Complete, Roche). Cell lysates were cleared of nuclei by centrifugation (15000 g, 15 min). Proteins were separated on 8-10% SDS-PAGE gels and transferred to a nitrocellulose membrane. Membranes were incubated with primary specific antibodies: anti-Dis3L2 (Nobus biologicals, NBP1-84740), anti-Eri1/THEX1 (Cell Signaling, #4049), anti-TUT4/ZCCHC11 (Pro Sci incorporated, 46-610), anti-TUT7/ZCCHC6 (Proteintech, 25196-1-AP), and anti-ezrin/radixin/moesin (ERMs) (90/3) (provided by Heinz Furthmayr, Stanford University, CA). Primary antibodies were used at 1:2000 dilution and peroxidase-conjugated secondary antibodies (goat anti-rabbit, ThermoFisher Scientific #31460; rabbit anti-goat, ThermoFisher Scientific #31402) at 1:5000. Chemoluminescence was measured with LAS-3000 (Fujifilm). Band intensities were quantified with Image Studio Lite (LI-COR Biosciences), normalized to ERMs values and relativized to unstimulated conditions (when no band was detected at 0 h, background was taken as reference signal).

QUANTIFICATION AND STATISTICAL ANALYSIS

MiRNA differential expression changes in miRNA-seq (n=3 donors) were considered significant when associated with a Benjamini-Hochberg adjusted p-value < 0.1. Kruskal-Wallis test and Dunn's multiple comparisons test were applied using GraphPad Prism to perform statistical analysis on western blot (n=8, 8 donors) and qPCR (n=9, 9 donors) data, representing in figures significance as: * p-value <0.05, ** p-value<0.01, *** p-value<0.001; 0.05<p-value<0.1: indicated with numbers. Ingenuity Pathway Analysis uses Fisher's Exact Test p-value with a threshold value 0.05, as stated in the figure legend.

All graphs (except: heatmaps, Venn diagram, miRNet networks and Chimira global profile) were plotted using GraphPad Prism, therefore, for detailed definitions of measures such as mean, median or SEM, program online guides can be reviewed.